



# Semihydrogenation of phenylacetylene over nonprecious Ni-based catalysts supported on AISBA-15

Lei Yang<sup>a</sup>, Shiyi Yu<sup>a</sup>, Chong Peng<sup>b</sup>, Xiangchen Fang<sup>b,\*</sup>, Zhenmin Cheng<sup>a</sup>, Zhiming Zhou<sup>a,\*</sup>

<sup>a</sup> State Key Laboratory of Chemical Engineering, East China University of Science and Technology, Shanghai 200237, China

<sup>b</sup> Fushun Research Institute of Petroleum and Petrochemicals, SINOPEC, Fushun 113001, China



## ARTICLE INFO

### Article history:

Received 18 December 2018

Accepted 9 January 2019

### Keywords:

Semihydrogenation

Phenylacetylene

Nonprecious catalyst

Structure-activity/selectivity

Alloy

Geometric and electronic effects

## ABSTRACT

A series of nonprecious monometallic Ni/AISBA-15 and bimetallic Ni–M (M = Zn, Ga, Cu, or Fe)/AISBA-15 catalysts were prepared using a urea precipitation method and applied to the semihydrogenation of phenylacetylene. The catalysts were characterized by various techniques, showing that the Ni particle size of catalyst can be tuned by adjusting the Al content, and NiZn and NiGa supported catalysts exhibited geometric and electronic effects that originated from the bimetallic alloy. Among all the catalysts studied, NiZn<sub>3</sub>/AISBA-15, with a turnover frequency of 10.89 s<sup>-1</sup> comparable to that of precious Pd-based catalysts, presented the highest selectivity to styrene (90.3%) at nearly 100% conversion of phenylacetylene in semibatch operation. This catalyst was further evaluated in a continuous fixed-bed reactor for semihydrogenation of a model C<sub>8</sub> aromatic fraction of pyrolysis gasoline (a mixture of phenylacetylene, styrene, ethylbenzene and xylene), which aimed at assessing its practical application of recovering styrene from pyrolysis gasoline. The results showed that at complete conversion of phenylacetylene, the styrene concentration in the product was always kept at a stable level and higher than its initial concentration over 100 h of time on stream, demonstrating high selectivity and good stability of NiZn<sub>3</sub>/AISBA-15. Finally, the application of NiZn<sub>3</sub>/AISBA-15 was extended to other phenylacetylene derivatives.

© 2019 Elsevier Inc. All rights reserved.

## 1. Introduction

As an important chemical monomer, styrene has been widely used for producing synthetic rubbers and plastics such as styrene-butadiene rubber, polystyrene and ABS resin. Styrene is mainly obtained by catalytic dehydrogenation of ethylbenzene, epoxypropane-styrene co-production and extraction of pyrolysis gasoline (pygas, byproduct of steam cracking of naphtha) [1–4]. In recent years, pygas extraction has attracted much attention from both academic and industrial researchers, because a 1Mt/a of steam cracking plant can produce about 24–42 kt/a of styrene [2,4]. However, unfortunately, phenylacetylene always exists in the styrene-containing feedstock, and even a small amount of phenylacetylene will poison the catalyst used in the polymerization process [3–6]. Considering the similar chemical structures of phenylacetylene and styrene, it is very difficult to separate them from one another. The most effective way to eliminate phenylacetylene from styrene is through the semihydrogenation reaction, which aims at completely converting phenylacetylene while

avoiding hydrogenation of styrene. Indeed, in the pygas extraction process, the feedstock sent to the extraction distillation unit is a hydrogenated C<sub>8</sub> stream composed mainly of aromatics, which is obtained by fractionating a pygas first and then hydrogenating any acetylenic compounds [1,2].

At present, Pd supported catalysts are most widely used for semihydrogenation of phenylacetylene due to the excellent activity at mild reaction conditions. However, the selectivity to styrene decreases quickly once the conversion of phenylacetylene exceeds 95%, which inevitably results in loss of styrene [7–13]. Moreover, the limited availability and high cost of Pd metal restrict the practical application of Pd catalysts. In this respect, it is urgent and important to develop less expensive catalysts with high activity and selectivity for semihydrogenation of phenylacetylene.

Among various nonprecious metal catalysts such as Ni [14–20], Fe [21] and Mo [22], Ni supported catalysts are mostly studied for phenylacetylene hydrogenation. For instance, Erokhin et al. [18] synthesized a Ni@C nanocomposite that exhibited around 60% selectivity to styrene at complete conversion of phenylacetylene; Golubina et al. [20] prepared a Ni/nanodiamond catalyst that showed 75% selectivity to styrene at 60% conversion of phenylacetylene, and the selectivity seemed to decrease with increasing the conversion although the results at a higher conversion was not

\* Corresponding authors.

E-mail addresses: [fangxiangchen.fshy@sinopec.com](mailto:fangxiangchen.fshy@sinopec.com) (X. Fang), [zmzhou@ecust.edu.cn](mailto:zmzhou@ecust.edu.cn) (Z. Zhou).

reported. After modifying Ni with P or Si to form nickel silicides [15,16,19,23] or nickel phosphides [24,25], the selectivity to styrene at nearly 100% conversion of phenylacetylene was increased to some extent, e.g., about 80% selectivity at 99% conversion for  $\text{Ni}_2\text{Si/SBA-15}$  [23] and 88.2% selectivity at 98.6% conversion for  $\text{Ni}_2\text{P/Al}_2\text{O}_3$  [25]. However, the modified catalysts in general had yet to show an acceptable selectivity up to 90% at complete conversion of phenylacetylene.

It is known in the literature that introduction of a second metal such as Cu [11,12], Zn [11,12] and Ga [26] to Pd can effectively improve the selectivity to styrene at high conversion of phenylacetylene. This strategy has been tried recently for Ni-based catalysts in spite of few studies available. Li et al. [27] prepared several supported Ni-Ga intermetallic compounds via an in situ reduction of layered double hydroxide (LDH) precursors, and the best catalyst displayed around 72% selectivity at nearly 100% conversion. Liu et al. [28] synthesized  $\text{Ni}_3\text{Ga/MgAl}_2\text{O}_4$  and  $\text{Ni}_3\text{Sn/MgAl}_2\text{O}_4$  nanocrystal catalysts that exhibited, respectively, 87% and 89% selectivity at >99% conversion. Very recently, Liu et al. [29] reported 90.3% selectivity at 95.8% conversion over a LDH-derived Ni-Cu nanoalloy catalyst, but the selectivity at almost 100% conversion was not presented. It is clear that, as mentioned above, the selectivity to styrene at nearly complete conversion of phenylacetylene needs to be improved. In addition, worthy of mention is that, to date, most of the catalysts reported in the literature have been tested using a model feedstock composed of phenylacetylene and solvent such as methanol and n-hexane, which is different from the practical situation where phenylacetylene is present in excess of styrene [2,22]. In such a case it is unclear whether the catalysts were still effective in removing phenylacetylene and preserving styrene owing to the competitive adsorption of phenylacetylene and styrene over the active sites of catalyst [4].

In this study, a series of monometallic Ni/AlSBA-15 and bimetallic Ni-M (M = Zn, Ga, Cu, or Fe)/AlSBA-15 nonprecious catalysts with varying Si/Al atomic ratio were prepared by a urea precipitation method and applied to the semihydrogenation of phenylacetylene. The structure- activity/selectivity relationships of these catalysts were explored and discussed. The best catalyst identified was assessed in the hydrogenation of model  $\text{C}_8$  aromatic fraction of pygas (a mixture of phenylacetylene, styrene, ethylbenzene and xylene) for 100 h in a fixed-bed reactor to simulate the practical application. Moreover, the semihydrogenation of other phenylacetylene derivatives was attempted.

## 2. Materials and methods

### 2.1. Preparation of Ni-based AlSBA-15 catalysts

The ordered mesoporous support AlSBA-15 was prepared by a modified technique of Vinu et al. [30]. First, 30 g of deionized water and 70 g of  $0.28 \text{ mol}\cdot\text{L}^{-1}$  hydrochloric acid (36–38%, Sinopharm) were mixed at 40 °C, and then 4.0 g of Pluronic P123 ( $M_{\text{av}} = 5800$ , Sigma-Aldrich) was added with stirring until the P123 was completely dissolved. Next, 9.0 g of tetraethyl orthosilicate ( $\geq 98\%$ , Sinopharm) and a predetermined amount of aluminium isopropoxide ( $\geq 99\%$ , Sinopharm) were added with the trace injection pump under slowly stirring for 24 h at 40 °C, after which the solution was transferred to a Teflon-lined stainless-steel autoclave and heated at 110 °C for 24 h. Finally, the precipitate was filtered, washed successively with deionized water and ethanol ( $\geq 99.7\%$ , Sinopharm), dried at 80 °C for 10 h, and calcined at 550 °C for 6 h at a heating rate of  $1 \text{ }^\circ\text{C}\cdot\text{min}^{-1}$ . For simplicity, the as-prepared support was denoted as AlSBA-15(x), where x (x = 5, 10, 20, 40 or 80) represented the nominal Si/Al atomic ratio. For comparison, SBA-15

was also prepared using the same method except for without the addition of aluminum precursor.

Ni-based monometallic and bimetallic supported catalysts were prepared by a urea precipitation method [31,32]. A typical procedure was as follows: first, predetermined amounts of nickel nitrate ( $\text{Ni}(\text{NO}_3)_2\cdot 6\text{H}_2\text{O}$ ,  $\geq 99\%$ , Sinopharm) and M (M = Zn, Ga, Fe or Cu)-bearing nitrate ( $\text{Zn}(\text{NO}_3)_2\cdot 6\text{H}_2\text{O}$ ,  $\geq 99\%$ , Sinopharm;  $\text{Ga}(\text{NO}_3)_3\cdot \text{H}_2\text{O}$ , 99.99%, Sigma-Aldrich;  $\text{Fe}(\text{NO}_3)_3\cdot 9\text{H}_2\text{O}$ , 99%, Sinopharm;  $\text{Cu}(\text{NO}_3)_2\cdot 3\text{H}_2\text{O}$ , 99%, Sinopharm) and 0.5 g of SBA-15 or AlSBA-15(x) were added to 15 g of deionized water and stirred at room temperature for 1 h; next, 0.23 g of urea ( $\geq 99\%$ , Sinopharm) was added to the above solution and stirred at 90 °C for 15 h; finally, the suspension was filtered, washed with water, dried at 110 °C for 10 h, and calcined at 500 °C for 5 h at a heating rate of  $2 \text{ }^\circ\text{C}\cdot\text{min}^{-1}$ . Note that the M-bearing nitrate was added only for  $\text{NiM}_y/\text{AlSBA-15}$  catalysts, where y represented the nominal M/Ni atomic ratio; moreover, the nominal total metal loading (Ni + M) was kept at 10 wt%.

### 2.2. Catalyst characterization

The Brunauer-Emmett-Teller (BET) surface area ( $S_{\text{BET}}$ ), pore volume ( $V_{\text{pore}}$ ) and pore diameter ( $d_{\text{pore}}$ ) of samples were determined by  $\text{N}_2$  adsorption-desorption data collected at  $-196 \text{ }^\circ\text{C}$  on Micromeritics ASAP 2010. Before analysis the samples were degassed at 133 Pa and 200 °C for 6 h. Powder X-ray diffraction (XRD) on Rigaku D/Max 2550 was conducted to confirm the crystalline structure of sample by using a Cu K $\alpha$  radiation ( $\lambda = 0.15406 \text{ nm}$ ) in the range of  $2\theta = 0.5\text{--}5^\circ$  and  $10\text{--}80^\circ$  at a scan rate of  $0.02^\circ\cdot\text{s}^{-1}$ . Inductively coupled plasma-optical emission spectroscopy (ICP-OES) was performed on Varian 710-ES to detect the actual composition and metal loading of catalyst. High-resolution transmission electron microscopy (HRTEM) was recorded on JEOL JEM-2100 to observe the morphology and the metal particle size of catalyst. Temperature-programmed reduction (TPR) of catalyst was carried out on Micromeritics AutoChem 2920 to investigate the metal-support interaction. The sample was reduced from room temperature to 800 °C in 10%  $\text{H}_2/\text{Ar}$  at a heating rate of  $10 \text{ }^\circ\text{C}\cdot\text{min}^{-1}$ , and the  $\text{H}_2$  consumption was monitored by a thermal conductivity detector (TCD). The amount of active sites of Ni-based catalysts were also acquired on this instrument by CO pulse chemisorption, assuming the chemisorption stoichiometry of  $\text{CO}:\text{Ni} = 1$ . The catalyst was first *in situ* reduced at 800 °C for 2 h in 10%  $\text{H}_2/\text{Ar}$  at a heating rate of  $10 \text{ }^\circ\text{C}\cdot\text{min}^{-1}$ , followed by switching to He at 830 °C for 30 min to remove adsorbed  $\text{H}_2$ . After that, the catalyst was cooled to room temperature in He, and pulsed by CO until the CO peak area remained constant. The CO uptakes were monitored by TCD and calculated based on the accumulated adsorbed CO. X-ray photoelectron spectroscopy (XPS) was investigated on Thermo Scientific ESCALAB 250 Xi to analyze the surface electronic states of catalyst by using an Al K $\alpha$  radiation ( $h\nu = 1486.6 \text{ eV}$ ) and a pass energy of 40 eV, and the binding energies of spectra were referenced by C 1 s (284.8 eV).

### 2.3. Catalyst test

The semihydrogenation of phenylacetylene over various catalysts was carried out in a semibatch stirred tank reactor (300 mL, Parr 5100). First, 5 g of phenylacetylene (>98%, Alfa Aesar), 5 g of n-octane ( $\geq 98\%$ , Sinopharm) acting as internal standard, 90 g of methanol as solvent, and 0.15 g of pre-reduced catalyst (reduced at 800 °C for 2 h in 10%  $\text{H}_2/\text{N}_2$  at a heating rate of  $10 \text{ }^\circ\text{C}\cdot\text{min}^{-1}$ ) were added into the reactor, and the mixture was heated to 40 °C in  $\text{N}_2$ . Next,  $\text{H}_2$  was charged into the reactor to purge  $\text{N}_2$  for several times. Finally, the reaction occurred at 40 °C and 0.1 MPa in  $\text{H}_2$  with vigorous stirring at 1000 rpm. A small amount of liquid product (around 1 mL) was withdrawn from the reactor in a certain interval

and analyzed by gas chromatography (GC) using an HP 6890 GC system equipped with a capillary column (PEG-20 M, 30 m × 0.32 mm × 0.50 μm) and a flame ionization detector.

The best catalyst identified from screening all catalysts was further applied to a continuous operation system, where H<sub>2</sub> and a simulated C<sub>8</sub> aromatic fraction of pygas (a mixture of 2 wt% of phenylacetylene, 28 wt% of styrene (>99%, Alfa Aesar), 30 wt% of ethylbenzene (>99%, Sinopharm) and 40 wt% of xylene (>99%, Sinopharm) [2,4]) flowed concurrently downwards through a fixed-bed reactor (height: 20 cm; inner diameter: 1 cm), as shown in Fig. S1. 1 g of catalyst (40–60 mesh) was loaded at the middle of the reactor, and the upper and lower parts of the reactor were filled with glass beads (40–60 mesh). The reaction temperature was adjusted by hot water circulating through the reactor jacket and the pressure was controlled by a back-pressure regulator. The gas and liquid flow rates entering the reactor were controlled by mass flow controller and HPLC metering pump, respectively. The product was withdrawn through a six-way valve located at the outlet of the reactor. The operating conditions were as follows: temperature (*T*), 40–90 °C; pressure (*P*), 0.2–1.0 MPa; liquid flow rate (*F<sub>L</sub>*, accurately controlled by a metering pump), 0.05–0.3 mL·min<sup>-1</sup>; H<sub>2</sub> flow rate (*F<sub>C</sub>*), 10 NmL·min<sup>-1</sup>. The stability of the best catalyst was evaluated in 100 h of reaction under an optimal condition.

Finally, the best catalyst was applied to the semihydrogenation reaction of other phenylacetylene derivatives, including 4-methylphenylacetylene (>99%, Alfa Aesar), 4-methoxyphenylacetylene (>99%, Alfa Aesar), 4-chlorophenylacetylene (>98%, Alfa Aesar), and 3-aminophenylacetylene (>99%, Alfa Aesar). The reaction was conducted at 40 °C and 0.1 MPa in the stirred tank reactor. The amounts of reactant, solvent (methanol), internal standard (n-octane) and catalyst are the same as those used in the semihydrogenation of phenylacetylene.

Conversion of phenylacetylene is defined as moles of phenylacetylene consumed divided by initial phenylacetylene moles. Selectivity to styrene is defined as moles of styrene produced per mole of phenylacetylene consumed. The catalyst activity is expressed in terms of the initial rate and the turnover frequency (TOF), with the former defined as moles of phenylacetylene con-

verted per gram of catalyst per second during the initial period, and the latter as moles of phenylacetylene converted per mole of active sites per second. The TOF values were calculated as follows:

$$\text{TOF} = \frac{F\alpha}{tWN} \quad (1)$$

where *F* is the mole of phenylacetylene in the feedstock, mole;  $\alpha$  is the conversion of phenylacetylene; *t* is the reaction time, s; *W* is the catalyst weight, g; and *N* is the mole of Ni active sites determined by CO chemisorption, mol·g<sup>-1</sup>. Note that the conversion data used for calculating the TOF values are lower than 30%.

### 3. Results and discussion

#### 3.1. Effect of Al doping

The ordered mesoporous structures of SBA-15 and AISBA-15 are confirmed by small-angle XRD and HRTEM analysis (Fig. S2). In addition, for AISBA-15, the incorporation and coordination of aluminum atoms into the framework of SBA-15 is evidenced by small-angle XRD. The BET surface area, pore volume, average pore diameter and actual Si/Al atomic ratio of the support materials are listed in Table 1. For AISBA-15(x), the actual Si/Al atomic ratios ranging from 839 to 23 are much larger than the corresponding nominal ratios from 80 to 5, which might be attributed to the high solubility of the Al precursor (aluminium isopropoxide) in the acidic medium [30]. With increasing the Al content or decreasing the Si/Al ratio, the BET surface area of support increases first, passes through a maximum (955.4 m<sup>2</sup>·g<sup>-1</sup> for AISBA-15(40)), and then decreases monotonically. This variation is in accordance with previous work by Vinu et al. [30,33]: the increase in surface area is probably due to the incorporation of Al atoms into SBA-15 structure, while the decrease is attributed to the possible presence of aluminum oxide species inside and outside the mesopores of support as a result of increased Al content. The presence of mesopores in AISBA-15(x) is evidenced by the N<sub>2</sub> adsorption-desorption isotherms and the pore-size distribution curves (Fig. S3). In addition,

**Table 1**  
Physicochemical properties of supports and catalysts.

Catalysts	S <sub>BET</sub> <sup>a</sup> (m <sup>2</sup> /g)	V <sub>pore</sub> <sup>a</sup> (cm <sup>3</sup> /g)	d <sub>pore</sub> <sup>a</sup> (nm)	n <sub>Si</sub> /n <sub>Al</sub> <sup>b</sup>	Metal loading <sup>c</sup> (wt%)		Particle size <sup>d</sup> (nm)	CO uptake (μmol·g <sup>-1</sup> cat)	Initial rate <sup>e</sup> (μmol·g <sup>-1</sup> cat·s <sup>-1</sup> )	TOF <sup>e</sup> (s <sup>-1</sup> )
					Ni	M				
SBA-15	775.2	1.09	6.0	–	–	–	–	–	–	–
AISBA-15(80)	861.6	1.13	6.3	839	–	–	–	–	–	–
AISBA-15(40)	955.4	1.21	6.4	365	–	–	–	–	–	–
AISBA-15(20)	823.8	1.20	6.7	219	–	–	–	–	–	–
AISBA-15(10)	778.6	1.18	6.8	117	–	–	–	–	–	–
AISBA-15(5)	578.6	1.32	9.3	23	–	–	–	–	–	–
Ni/SBA-15	400.8	1.03	9.7	–	8.3	–	5.3	1.73	8.26	4.78
Ni/AISBA-15(80)	505.7	1.04	8.6	839	7.9	–	4.2	1.86	8.64	4.65
Ni/AISBA-15(40)	533.7	1.07	9.1	365	8.5	–	3.3	2.43	10.76	4.42
Ni/AISBA-15(20)	399.8	1.02	9.5	219	8.6	–	6.3	1.42	6.92	4.87
Ni/AISBA-15(10)	397.9	1.05	9.9	117	8.1	–	7.3	1.23	7.17	5.83
Ni/AISBA-15(5)	322.0	1.21	10.2	23	8.1	–	7.8	1.01	6.30	6.24
NiCu <sub>0.6</sub> /AISBA-15(40)	257.3	0.53	8.2	365	4.9	3.3	2.6	2.18	8.95	4.11
NiGa <sub>0.6</sub> /AISBA-15(40)	513.2	1.02	8.7	365	5.1	3.5	6.5	0.92	6.38	6.93
NiFe <sub>0.6</sub> /AISBA-15(40)	387.5	1.23	12.7	365	4.9	2.8	15.1	0.61	2.64	4.32
NiZn <sub>0.6</sub> /AISBA-15(40)	532.3	1.07	9.1	365	5.3	3.1	4.2	1.78	7.57	4.25
NiZn <sub>1.5</sub> /AISBA-15(40)	335.5	0.78	9.4	365	3.2	5.3	7.2	0.73	6.19	8.47
NiZn <sub>3</sub> /AISBA-15(40)	376.6	0.98	10.4	365	1.8	6.1	7.5	0.41	4.47	10.89
NiZn <sub>5</sub> /AISBA-15(40)	331.8	0.84	10.1	365	1.2	6.8	8.2	0.23	2.16	9.43

<sup>a</sup> Calculated from the desorption branch of the N<sub>2</sub> physisorption isotherm by the BJH method.

<sup>b</sup> Actual Si/Al atomic ratio determined by the ICP-OES analysis.

<sup>c</sup> Actual metal loading determined by the ICP-OES analysis.

<sup>d</sup> Average metal particle size determined by the HRTEM analysis using at least 100 particles.

<sup>e</sup> Calculated using the conversion data lower than 30%.

it is noticed that the hysteresis loops of the isotherms shift to higher relative pressure with increasing the Al content, and accordingly, resulting in larger pore size.

The  $N_2$  adsorption-desorption isotherms of Ni/SBA-15 and Ni/AISBA-15(x) catalysts (Fig. 1) display typical hysteresis loops of mesoporous materials, implying that the mesoporous structure of support is preserved after introduction of Ni particles. In addition, the  $N_2$  sorption hysteresis loop of Ni/AISBA-15(x) shifts to higher relative pressure as compared to that of AISBA-15(x), indicating a larger pore size of catalyst. As presented in Table 1, the average pore diameter of Ni/AISBA-15(x) is around 1.4 times that of the corresponding AISBA-15(x). On the contrary, all Ni/AISBA-15(x) have BET surface areas much smaller than their support counterparts, suggesting deposition of nickel species on AISBA-15 [32]. It is worthy of note that the variation of BET surface area with the Al content for Ni/AISBA-15(x) follows the same trend as observed for the support materials. Among all Ni/AISBA-15(x), Ni/AISBA-15(40) has the largest surface area. Around 80% of nickel species is deposited on AISBA-15 (actual Ni loadings of 7.9–8.6 wt%, Table 1), showing the effectiveness of the urea precipitation method used here for preparing catalysts.

Fig. 2 shows the XRD patterns of reduced Ni/AISBA-15(x). The well-preserved characteristic peaks in the small-angle range imply that the ordered mesoporous structure of AISBA-15 is maintained. Compared to AISBA-15(x) (Fig. S2), the (1 0 0) plane peak of Ni/AISBA-15(x), especially those catalysts with  $x \geq 20$ , shifts to a smaller angle, indicating the incorporation of Ni species into the framework of AISBA-15 (the bond length of Ni–O (1.93–2.07 Å) is longer than those of Si–O and Al–O bonds) [32,34,35]. However, for Ni/AISBA-15(10) and Ni/AISBA-15(5), this angle shift is very small by comparison of Ni/AISBA-15(10) and AISBA-15(10) (or Ni/AISBA-15(5) vs AISBA-15(5)), which is probably due to the aforementioned presence of excess  $Al_2O_3$  that prevents Ni from being incorporated into AISBA-15. The broad peaks at  $2\theta = 44.5$  and  $51.8^\circ$  are assigned to (1 1 1) and (2 0 0) planes of metallic  $Ni^0$  (JCPDS 04-0850), respectively. The intensity of these peaks decreases first and then increases with the Al content, meaning that the crystallite size of Ni can be tuned by adjusting the Al content. Among all Ni/AISBA-15(x), the Ni crystallite size of Ni/AISBA-15(40) seems to be the smallest.

Fig. 3 shows the  $H_2$ -TPR profiles of Ni/AISBA-15(x). There exits only one broad reduction peak centered at around  $600^\circ C$  for each catalyst, which belongs to the strong metal-support interaction [32]. Like the BET surface area and the intensity of  $Ni^0$  characteris-

tic peak, the reduction peak temperature of Ni/AISBA-15(x) varies with the Al content: increases first, and then decreases, with the highest reduction peak temperature of  $610^\circ C$  for Ni/AISBA-15(40). The higher reduction temperature or the stronger metal-support interaction is closely associated with the incorporation of Ni into AISBA-15 that makes the reduction of  $NiO$  species difficulty. However, with a further increase in the Al content, the amount of Ni incorporated into AISBA-15 decreases, as reflected by the XRD analysis, and consequently it is relatively easy to reduce the catalysts such as Ni/AISBA-15(10) and Ni/AISBA-15(5).

Fig. 4 displays the HRTEM images and the corresponding Ni particle size distributions of reduced Ni/AISBA-15(x) catalysts. All samples exhibit ordered mesoporous structures, which is in line with the XRD analysis. With increasing the Al content, the average Ni particle size of Ni/AISBA-15(x) varying between 3.3 and 7.8 nm first decreases and then increases, which is also in agreement with XRD. As shown in Table 1, a negative correlation is observed between the average Ni particle size and the CO uptake of Ni/

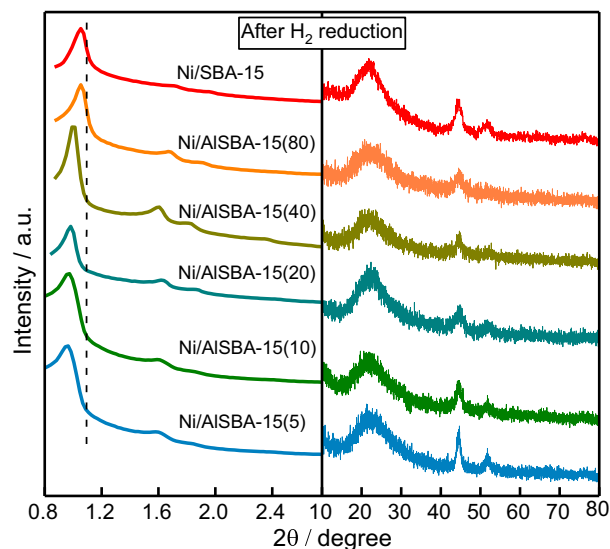


Fig. 2. XRD patterns of reduced Ni/AISBA-15(x) catalysts.

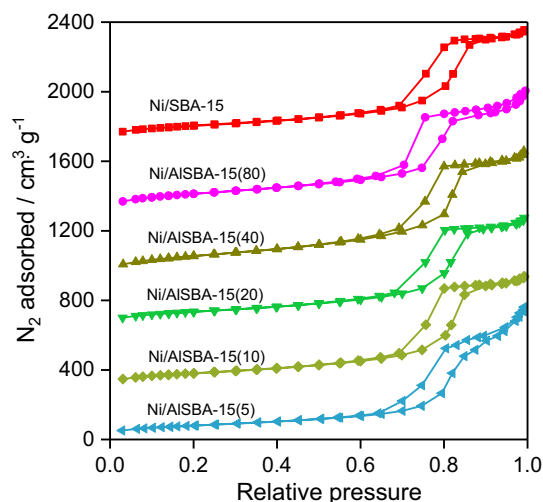


Fig. 1.  $N_2$  adsorption-desorption isotherms of Ni/AISBA-15(x) catalysts.

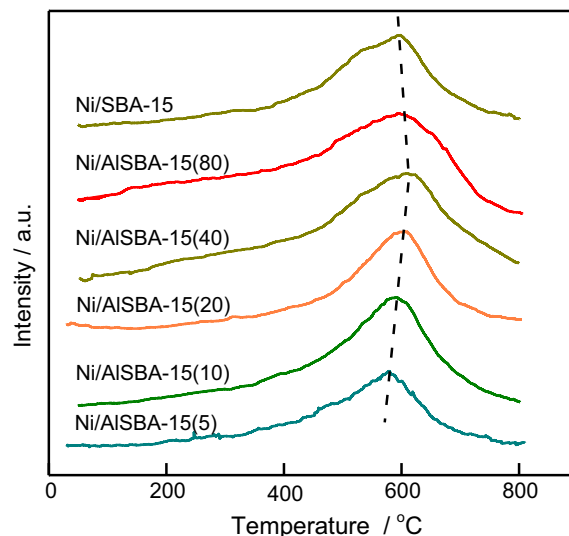
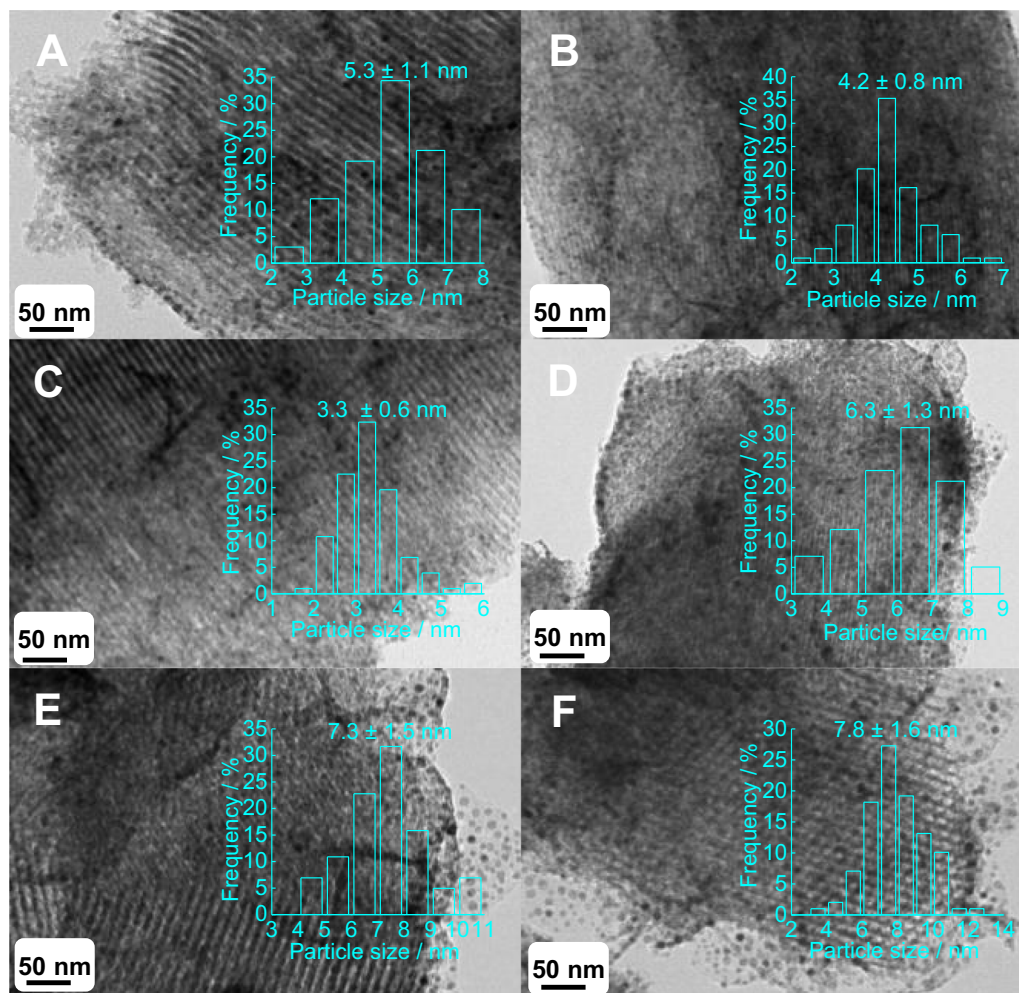


Fig. 3.  $H_2$ -TPR profiles of Ni/AISBA-15(x) catalysts.



**Fig. 4.** HRTEM images and the corresponding histograms of Ni particle size distribution of reduced Ni/AlSBA-15(x) catalysts: (A) Ni/SBA-15, (B) Ni/AlSBA-15(80), (C) Ni/AlSBA-15(40), (D) Ni/AlSBA-15(20), (E) Ni/AlSBA-15(10), and (F) Ni/AlSBA-15(5).

AlSBA-15(x), implying more active sites for the catalyst with smaller Ni particle size. In addition, compared to Ni/AlSBA-15(40) whose average Ni particle size (3.3 nm) is much smaller than the average pore diameter (9.1 nm), Ni/AlSBA-15(5) has comparable Ni particle size (7.8 nm) with the pore size (10.2 nm), indicating that many Ni particles of Ni/AlSBA-15(5) are deposited and aggregated on the outer surface of AlSBA-15(5).

Fig. 5 presents the XPS spectra of Ni 2p and Al 2p core levels of reduced Ni/AlSBA-15(40) and Ni/AlSBA-15(5). Deconvolution of the Ni 2p peaks (Fig. 5(a)) of both catalysts yields three separate peaks at the binding energies (BEs) of 852.7, 856.1, and 861.1 eV, which are assigned to Ni<sup>0</sup>, NiO and nickel satellite peak, respectively [36–39]. It should be stressed that there is no peak shift for Ni 2p peaks, indicating no electronic effect of Al on Ni. Deconvolution of the Al 2p spectrum of Ni/AlSBA-15(5) reveals two peaks at BEs of 74.4 and 75 eV (Fig. 5(b)), corresponding to the tetrahedral and octahedral aluminum states, respectively [40]. In the tetrahedral state, Al is covalently bound to four Si atoms via oxygen bridges, while in the octahedral state, Al is not incorporated into the SBA-15 framework and it exists in the form of aluminum oxide [33]. This finding confirms the presence of aluminum oxide on Ni/AlSBA-15(5), which in turn, as discussed above, gives rise to small BET surface area and large Ni particle size of the catalyst. As for Ni/AlSBA-15(40), the Al 2p spectrum is curve-fitted into only one peak at BE of 74.4 eV (Fig. 5(b)), indicative of incorporation of all Al into the SBA-15 framework.

The conversion-time and conversion-selectivity curves of Ni/AlSBA-15(x) in phenylacetylene hydrogenation are displayed in Fig. S4, and the corresponding initial rate and the turnover frequency (TOF) are listed in Table 1. The TOF values vary from 4.42 and 6.24 s<sup>-1</sup>, which are of the same order of magnitude as those (1.3–21.4 s<sup>-1</sup>) achieved using Pd-based catalysts under similar mild reaction conditions [3,8,11,12]. This demonstrates that non-precious Ni/AlSBA-15(x) can catalyze the phenylacetylene hydrogenation with a specific activity comparable to that exhibited by precious Pd-based catalysts. The TOFs show a positive correlation with the average Ni particle sizes, revealing that the phenylacetylene hydrogenation on nickel surface is a structure-sensitive reaction. This characteristic is also found on Pd-based catalysts [3,12,41]. Nevertheless, like the CO uptake, the initial rate in general has a negative correlation with the Ni particle size. Ni/AlSBA-15(40) has the highest initial rate and thus the highest apparent activity. As regards the selectivity to styrene at almost complete conversion of phenylacetylene (≥99.5%), Ni/SBA-15, Ni/AlSBA-15(80) and Ni/AlSBA-15(40) have similar selectivity of about 84.5% (Fig. S4), which is larger than that of Ni/AlSBA-15(20) (80.8%), Ni/AlSBA-15(15) (70.6%) and Ni/AlSBA-15(5) (62.7%). It appears that the selectivity to styrene remains unchanged with increasing the average Ni particle size of catalyst from 3.3 to 5.3 nm, but decreases with a further increase in Ni particle size (6.3–7.8 nm). This implies that smaller Ni particle size is favorable for increasing the selectivity to styrene.

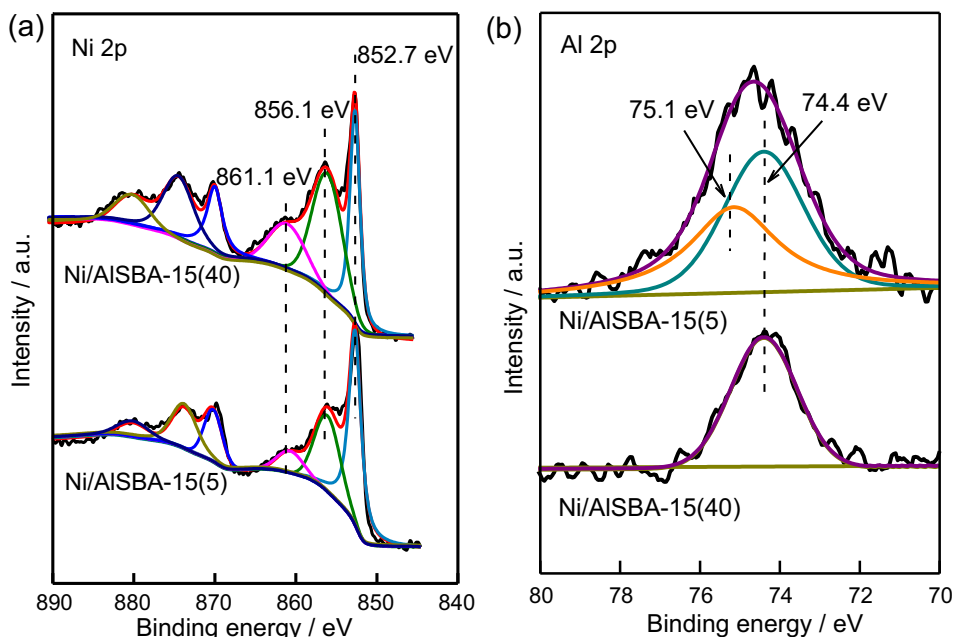


Fig. 5. XPS spectra of (a) Ni 2p and (b) Al 2p of reduced Ni/AISBA-15(40) and Ni/AISBA-15(5) catalysts.

There exists NiO on the surface of reduced catalyst according to the above XPS analysis, which we believe is mainly due to the oxidation of Ni<sup>0</sup> by air during sample transfer [29,32,42]. In addition, Ni instead of NiO is the predominant active phase for the semihydrogenation of phenylacetylene. This is because the unreduced NiO/AISBA-15(40) shows very low activity, with only 7.5% conversion of phenylacetylene after 500 min of reaction (Fig. S4). In contrast, the reduced Ni/AISBA-15(40) realizes 99.6% conversion in about 350 min. Considering that Ni/AISBA-15(40) has the highest apparent activity and the highest selectivity to styrene among all Ni/AISBA-15(x), it is selected as the reference catalyst in the next section to explore the activity and selectivity of bimetallic catalysts, namely, NiM/AISBA-15(40) (M = Zn, Ga, Fe or Cu).

### 3.2. Effect of second metal

Bimetallic NiM/AISBA-15(40) (M = Zn, Ga, Fe or Cu) catalysts with M/Ni atomic ratio of 0.6 are prepared. In addition, three NiZn<sub>y</sub>/AISBA-15(40) (y = 1.5, 3 and 5) are synthesized by taking into account the high performance of NiZn/MgAl<sub>2</sub>O<sub>4</sub> with a high molar ratio of Zn/Ni for the semihydrogenation of acetylene [43]. Supported NiGa, NiFe and NiCu catalysts with high molar ratios of M/Ni are not considered in this study because a relatively high amount of Ga [27], Cu [29] or Fe [44] was found to result in low selectivity. Like Ni/AISBA-15(x) whose actual Ni loading is about 8.0 wt%, the actual metal loadings (Ni + M) of NiCu<sub>0.6</sub>/AISBA-15(40), NiGa<sub>0.6</sub>/AISBA-15(40), NiFe<sub>0.6</sub>/AISBA-15(40), NiZn<sub>0.6</sub>/AISBA-15(40), NiZn<sub>1.5</sub>/AISBA-15(40), NiZn<sub>3</sub>/AISBA-15(40) and NiZn<sub>5</sub>/AISBA-15(40) are 8.2, 8.6, 7.7, 8.4, 8.5, 7.9 and 8.0 wt%, respectively (Table 1). The actual M/Ni atomic ratios of these catalysts are 0.62, 0.58, 0.60, 0.52, 1.49, 3.04 and 5.10, respectively, which are close to the nominal M/Ni atomic ratios. The existence of hysteresis loops in N<sub>2</sub> physisorption isotherms of bimetallic catalysts (Fig. S5) and the presence of characteristic diffraction peaks in small-angle XRD patterns (Fig. 6) taken together demonstrate that the ordered mesoporous structures still remain after introduction of the second metal.

The wide-angle XRD patterns of these catalysts are also illustrated in Fig. 6. NiGa<sub>0.6</sub>/AISBA-15(40) exhibits diffraction peaks

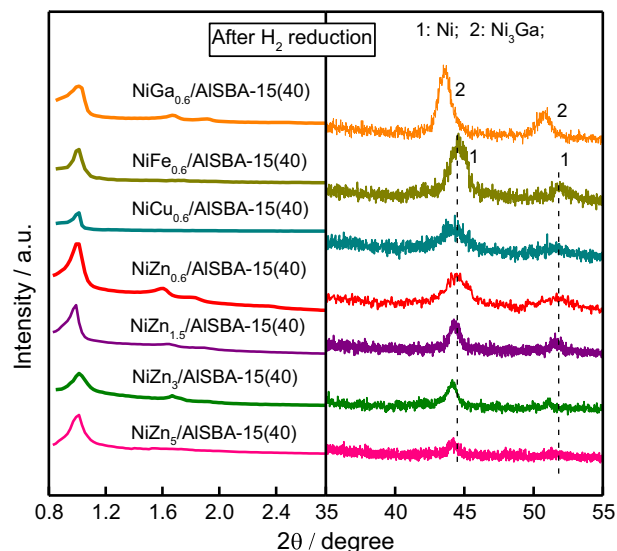


Fig. 6. XRD patterns of reduced bimetallic catalysts.

(2θ = 43.6 and 50.7°) belonging to Ni<sub>3</sub>Ga [27,28], indicating the formation of Ni–Ga alloy. NiCu<sub>0.6</sub>/AISBA-15(40), NiFe<sub>0.6</sub>/AISBA-15(40) and NiZn<sub>0.6</sub>/AISBA-15(40) show diffraction peaks (2θ = 44.5 and 51.8°) indexed to metallic Ni<sup>0</sup>. For the NiZn supported catalysts, with increasing the molar ratio of Zn/Ni, the peak at 44.5° shifts to smaller angles, which is located between 44.5° and 43.2° (the (1 0 1) plane of Zn) indicating the formation of Ni–Zn alloy [45,46]. The possible presence of Ni–Zn alloy is also reflected by the H<sub>2</sub>-TPR analysis (Fig. S6), from which it is found that the reduction peak gradually shifts from 630 °C to 690 °C with increasing the molar ratio of Zn/Ni from 0.6 to 5.0.

HRTEM and lattice images of reduced bimetallic catalysts demonstrate the alloy formation for NiGa<sub>0.6</sub>/AISBA-15(40), NiZn<sub>1.5</sub>/AISBA-15(40), NiZn<sub>3</sub>/AISBA-15(40) and NiZn<sub>5</sub>/AISBA-15(40) (Fig. 7). On the one hand, NiFe<sub>0.6</sub>/AISBA-15(40), NiZn<sub>0.6</sub>/AISBA-15(40) and NiCu<sub>0.6</sub>/AISBA-15(40) display small particles with a lattice

spacing of 0.203 nm (determined by fast Fourier transform pattern (FFT) (inset)), corresponding to the (1 1 1) plane of fcc Ni [31,47]. On the other hand, a lattice spacing of 0.206 nm is observed for NiGa<sub>0.6</sub>/AISBA-15 and a lattice spacing of 0.208 nm for NiZn<sub>1.5</sub>/AISBA-15(40), NiZn<sub>3</sub>/AISBA-15(40) and NiZn<sub>5</sub>/AISBA-15(40), which are assigned to the (1 1 1) plane of Ni-Ga alloy [27,48] and the (8 1 5) plane of Ni-Zn alloy (JCPDS card No. 47-1019), respectively. It is interesting that the Ni-Zn alloy is formed with increasing the Zn/Ni ratio. This result is consistent with the XRD analysis as mentioned above. The HRTEM-determined average metal particle size of bimetallic catalysts ranges from 2.6 to 15.1 nm, depending on the type of the second metal. Like monometallic Ni/AISBA-15(x), the bimetallic catalyst with a smaller metal particle size generally possesses higher CO uptake (Table 1). Note that NiZn<sub>3</sub>/AISBA-15(40) and NiZn<sub>5</sub>/AISBA-15(40) have metal particle sizes (7.5 and 8.2 nm, respectively) smaller than that of NiFe<sub>0.6</sub>/AISBA-15(40) (15.1 nm), but their CO uptakes (0.41 and 0.23 μmol · g<sub>cat</sub><sup>-1</sup>, respectively) are lower than that of NiFe<sub>0.6</sub>/AISBA-15(40) (0.61 μmol · g<sub>cat</sub><sup>-1</sup>), which could be attributed to the very low Ni loading of the two catalysts.

XPS analysis of reduced bimetallic catalysts further confirms the alloy formation for NiGa<sub>0.6</sub>/AISBA-15(40) and NiZn<sub>y</sub>/AISBA-15(40) (y = 1.5, 3 and 5). As illustrated in Fig. 8, among all NiM<sub>0.6</sub>/AISBA-15(40), only the Ni 2p<sub>3/2</sub> peak of NiGa<sub>0.6</sub>/AISBA-15(40) shifts to a lower BE (852.3 vs 852.7 eV), implying the electron transfer from Ga to Ni and the presence of electronic effect [27,28]. As for NiZn<sub>y</sub>/AISBA-15(40), the Ni 2p<sub>3/2</sub> peak gradually shifts negatively from 852.7 eV to 852.3 eV with increasing the molar ratio of Zn/Ni from 0.6 to 5.0, reflecting the electron transfer from Zn to Ni [49]. The above result clearly demonstrates that Ni atoms in NiGa<sub>0.6</sub>/AISBA-15(40) and NiZn<sub>y</sub>/AISBA-15(40) (y = 1.5, 3 and 5) are more electron-rich than those in other catalysts.

Fig. 9 shows the conversion-time and conversion-selectivity curves of the phenylacetylene hydrogenation over various bimetallic catalysts. Compared to monometallic Ni/AISBA-15(40), all bimetallic catalysts exhibit lower reaction rates, as indicated by more time required for about 100% conversion. Indeed, both the initial rate and the CO uptake of bimetallic catalysts (Table 1) are lower than those of Ni/AISBA-15(40), which is ascribed to the lower Ni loading of bimetallic catalyst. In addition, like monometallic catalysts, we observe a negative correlation between the initial rate and the metal particle size for bimetallic catalysts. By comparison of the TOF values for bimetallic catalysts and Ni/AISBA-15(40) (Table 1), it is found that the specific activity of Ni/AISBA-15(40) is slightly higher than those of NiZn<sub>0.6</sub>/AISBA-15, NiCu<sub>0.6</sub>/AISBA-15 and NiFe<sub>0.6</sub>/AISBA-15, but much lower than those of NiGa<sub>0.6</sub>/AISBA-15(40) and NiZn<sub>y</sub>/AISBA-15(40) (y = 1.5, 3 and 5), disclosing the positive effect of Ni–Ga and Ni–Zn alloy. In previous studies on Pd-based catalysts, some researchers also found that the alloy of Pd with a second metal can increase the hydrogenation activity of catalysts, e.g., the TOF value for benzene hydrogenation catalyzed by Pd–Rh/CNT was round 5 times higher than that of Rh/CNT and nearly 2 orders of magnitude higher than that of Pd/CNT [50], and the activity of Pd–Ru/PCNT catalyst in the selective hydrogenation of cinnamaldehyde to cinnamyl alcohol was superior to Pd/PCNT and Ru/PCNT [51].

As far as the selectivity and nearly 100% conversion is concerned, the bimetallic catalysts follow the order NiZn<sub>3</sub>/AISBA-15 (90.3%) > NiGa<sub>0.6</sub>/AISBA-15 (89.5%) > NiZn<sub>5</sub>/AISBA-15 (88.9%) > NiZn<sub>1.5</sub>/AISBA-15 (87.3%) > NiZn<sub>0.6</sub>/AISBA-15 (85.8%) > NiFe<sub>0.6</sub>/AISBA-15 (76.9%) > NiCu<sub>0.6</sub>/AISBA-15 (10.5%). The improved selectivity of NiZn<sub>y</sub>/AISBA-15 (y = 1.5, 3 and 5) and NiGa<sub>0.6</sub>/AISBA-15 as compared to Ni/AISBA-15(40) is mainly attributed to the electronic

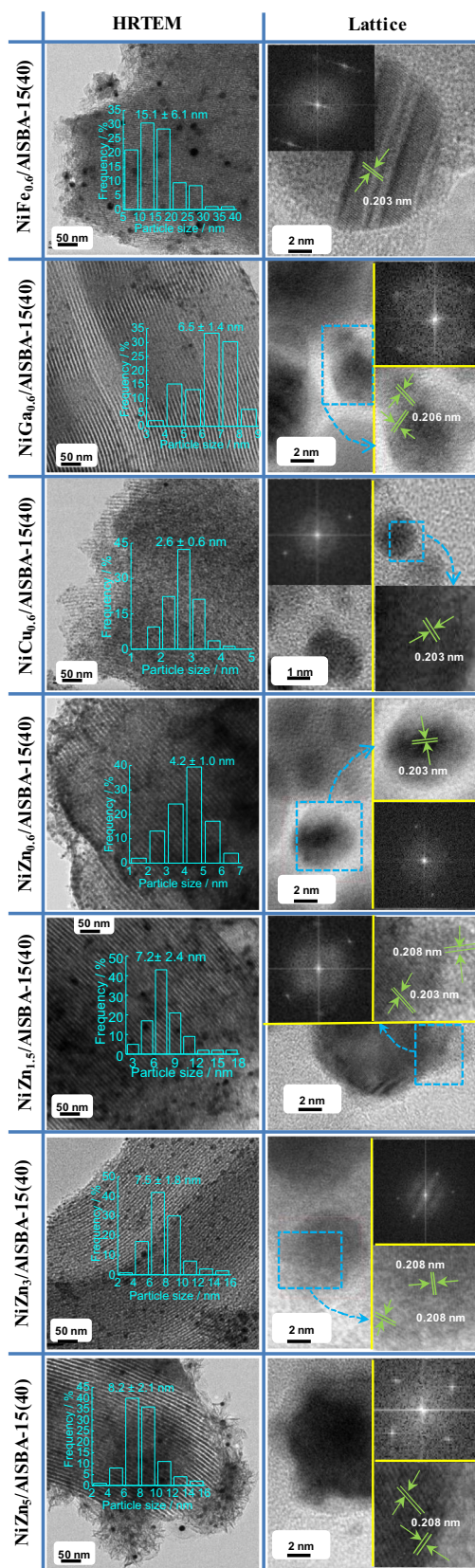


Fig. 7. HRTEM and lattice images of reduced bimetallic catalysts (the insets in the left and right panels show the corresponding histograms of metal particle size distribution and FFT spectra, respectively).

effect, because the electron-rich Ni active sites normally favor the desorption of electron-rich alkenes [7,52]. For example, Studt et al. [43] calculated the adsorption energy of ethylene on Ni(1 1 1) and

NiZn(1 1 1) planes, with the former about 0.2 eV lower than the latter, indicating that ethylene is more easily desorbed from the surface of NiZn. However, to date, most DFT calculations are performed on ethylene whose molecular size is smaller than that of styrene. Here, we calculate the adsorption energy of styrene on the metal active sites of Ni/AISBA-15(40), NiZn<sub>0.6</sub>/AISBA-15(40) and NiZn<sub>3</sub>/AISBA-15(40) (Fig. 10 and Fig. S7). The DFT calculation results show that the adsorption energies of styrene on the Ni(1 1 1) plane of Ni/AISBA-15(40), the Ni(1 1 1) plane of NiZn<sub>0.6</sub>/AISBA-15(40) and the NiZn<sub>3</sub>(8 1 5) plane of NiZn<sub>3</sub>/AISBA-15(40) are -2.03, -1.91 and -0.97 eV, respectively. The adsorption energy of styrene on NiZn<sub>3</sub>/AISBA-15(40) is much larger than that on Ni/AISBA-15(40) or NiZn<sub>0.6</sub>/AISBA-15(40), which means that styrene can readily desorb from the surface of NiZn alloy and thus avoid its over-hydrogenation into ethylbenzene.

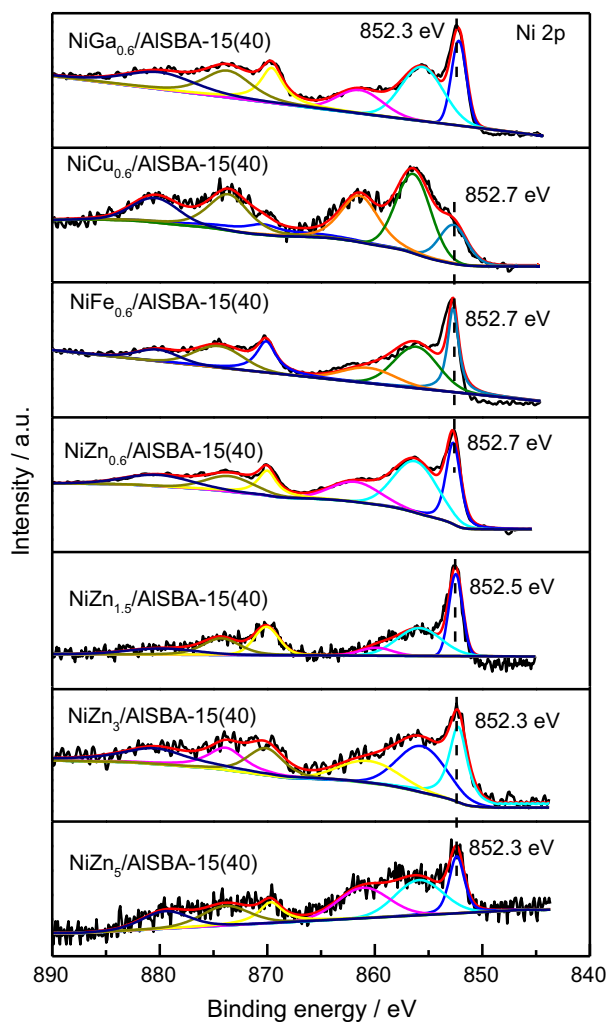


Fig. 8. XPS spectra of reduced bimetallic catalysts.

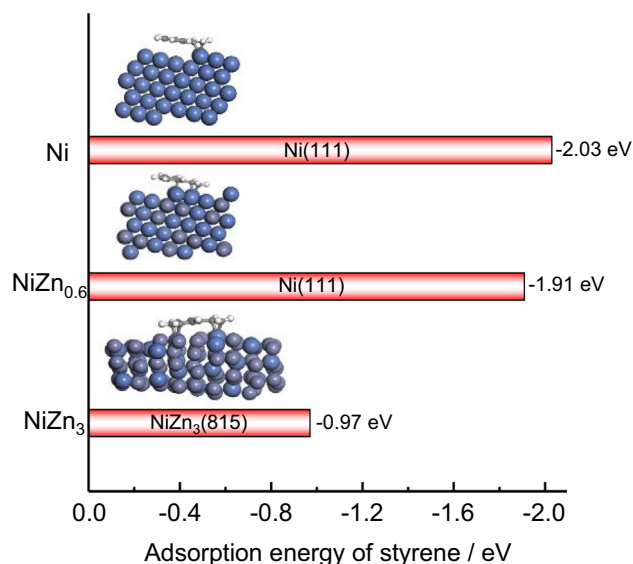


Fig. 10. Adsorption energies of styrene on the Ni(1 1 1) and NiZn(8 1 5) planes of different catalysts. (Ni, Zn, C and H atoms are modelled by dark blue, dark gray, gray and white, respectively.)

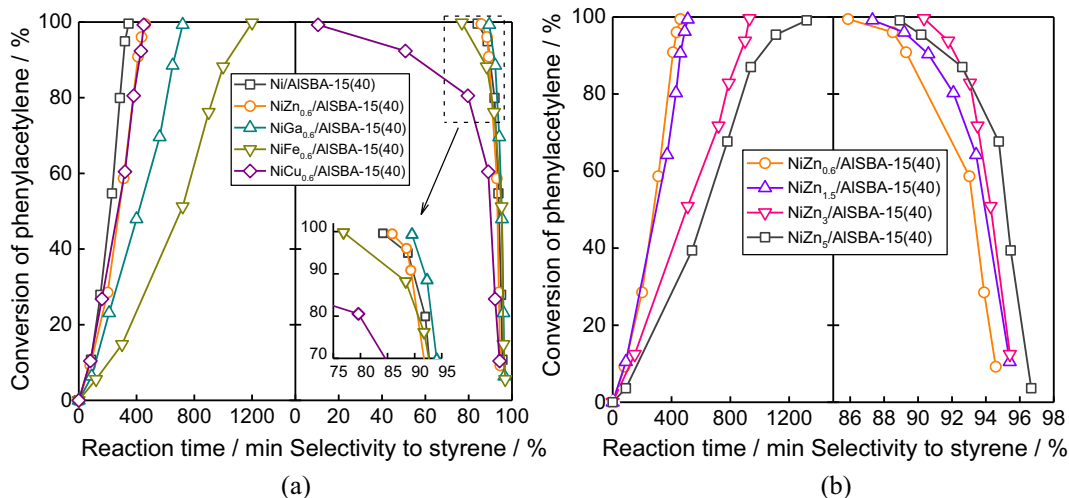


Fig. 9. Conversion vs time and selectivity curves over various bimetallic catalysts: (a) NiM<sub>0.6</sub>/AISBA-15(40) and (b) NiZn<sub>y</sub>/AISBA-15(40). (condition: 40 °C, 0.1 MPa, 5 wt% phenylacetylene in methanol, 0.15 g of catalyst and 100 g of solution in a semibatch stirred tank reactor).



### 3.3. Comparison with conventional catalysts

The above results show that NiZn<sub>3</sub>/AISBA-15(40) has the highest TOF value and the highest selectivity to styrene among all the catalysts investigated in this work. Next, NiZn<sub>3</sub>/AISBA-15(40) is compared with conventional catalysts used for semihydrogenation reactions. These catalysts include Pd-based catalysts (Pd/Al<sub>2</sub>O<sub>3</sub> and Lindlar catalyst) and Ni-based catalysts (Ni/Al<sub>2</sub>O<sub>3</sub> and Ni/SiO<sub>2</sub>), with the results listed in Table 2 and the conversion-time and conversion-selectivity curves presented in Fig. S8. As expected, Pd/Al<sub>2</sub>O<sub>3</sub> has the highest apparent activity, but with a low selectivity (47.8%) at 99.5% conversion. Lindlar catalyst, as a commercially widely used catalyst, shows a high selectivity (90.2%) at 99.3% conversion, but it takes about 20 times longer to reach the conversion than Pd/Al<sub>2</sub>O<sub>3</sub>, indicating low activity. Ni/Al<sub>2</sub>O<sub>3</sub> and Ni/SiO<sub>2</sub> exhibit much lower activity, with conversions of only 23.5% and 29.8%, respectively, after 900 min of reaction. In contrast, NiZn<sub>3</sub>/AISBA-15(40) gives rise to a high selectivity (90.3%) at 99.6% conversion with an acceptable activity (half of the time required for Lindlar catalyst to reach about the same conversion). In addition, by taking into account the relatively low cost of nonprecious Ni-based catalysts as compared to precious Pd-based catalysts, NiZn<sub>3</sub>/AISBA-15(40) is a potential catalyst for the semihydrogenation of phenylacetylene.

### 3.4. Application in semihydrogenation of model C<sub>8</sub> aromatic fraction of pygas

NiZn<sub>3</sub>/AISBA-15(40) is further evaluated in a continuous fixed-bed reactor for the semihydrogenation of model C<sub>8</sub> aromatic fraction of pygas, aiming at assessing its practical application of recovering styrene from pygas. Fig. S9 show the effects of temperature, pressure and liquid flow rate, from which the optimal reaction condition is determined as follows: *T* = 80 °C, *P* = 0.6 MPa, *F<sub>L</sub>* = 0.1 mL·min<sup>-1</sup> and *F<sub>C</sub>* = 10 NmL·min<sup>-1</sup>. Under the optimal condition, phenylacetylene is completely removed and meanwhile the styrene concentration in the product is kept at a stable level (2.41 mol·L<sup>-1</sup> on average) during 100 h of time on stream (Fig. 11). Moreover, the styrene concentration in the product is always higher than the initial concentration (2.37 mol·L<sup>-1</sup>, as indicated by the red dashed line), which indicates that the amount of styrene in the feedstock is not reduced but rather increased owing to the efficient conversion of phenylacetylene into styrene. In addition, the ordered mesoporous structure and the average metal particle size (7.0 nm) of the used NiZn<sub>3</sub>/AISBA-15(40) are well maintained; the chemical state of Ni<sup>0</sup> (852.3 eV) is unchanged; no metal leaching is detected (Ni and Zn loadings of the used catalyst measured by ICP-OES are 1.7 wt% and 6.0 wt%, respectively); and almost no coke deposition occurs (1.5 wt% coke determined by

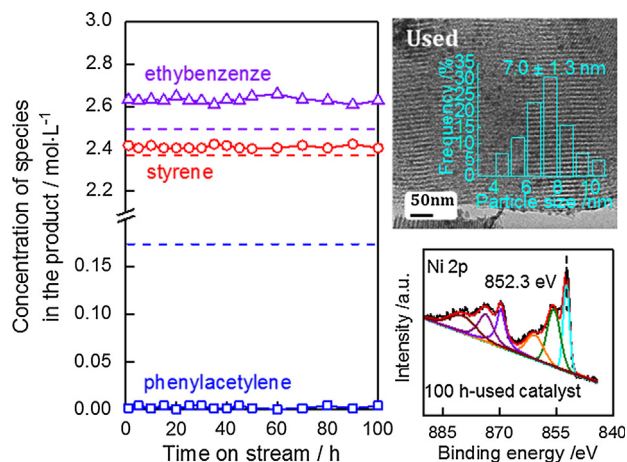


**Fig. 11.** Stability test of NiZn<sub>3</sub>/AISBA-15(40) in the semihydrogenation of model C<sub>8</sub> aromatic fraction of pygas (feedstock: 2 wt% of phenylacetylene (0.17 mol·L<sup>-1</sup>), 28 wt% of styrene (2.37 mol·L<sup>-1</sup>), 30 wt% of ethylbenzene (2.49 mol·L<sup>-1</sup>) and 40 wt% of xylene (3.32 mol·L<sup>-1</sup>); condition: *T* = 80 °C, *P* = 0.6 MPa, *F<sub>L</sub>* = 0.1 mL·min<sup>-1</sup> and *F<sub>C</sub>* = 10 NmL·min<sup>-1</sup>; in a continuous fixed-bed reactor). The dashed lines represent the concentration of species in the feedstock. The HRTEM and XPS analysis are performed on the 100 h-used NiZn<sub>3</sub>/AISBA-15(40).

thermogravimetric analyzer). Therefore, NiZn<sub>3</sub>/AISBA-15(40) is a promising catalyst for the semihydrogenation of C<sub>8</sub> aromatic fraction of pygas aiming at minimizing the concentration of phenylacetylene while maximizing the concentration of styrene.

### 3.5. Extension to semihydrogenation of phenylacetylene derivatives

Finally, the scope of NiZn<sub>3</sub>/AISBA-15(40) is extended to various phenylacetylene derivatives with different functional groups at the para- and meta-position of the alkyne group. The results are summarized in Table 3 and the conversion-time and conversion-selectivity curves are given in Fig. S10. Although the reaction rates vary depending on the type of phenylacetylene derivative (different time required for complete conversion), a high selectivity to the intermediate product (>90%) is attained for every reaction. This demonstrates that NiZn<sub>3</sub>/AISBA-15(40) can be extended to the semihydrogenation of many phenylacetylene derivatives.

## 4. Conclusions

Nonprecious monometallic Ni/AISBA-15 and bimetallic Ni-M/AISBA-15 (M = Zn, Ga, Cu, or Fe) were successfully prepared by a urea precipitation method, with the metal loading of about 8.0 wt% as determined by ICP-OES. The ordered mesoporous structure of the catalysts was evidenced by small-angle XRD, N<sub>2</sub> physisorption and HRTEM analyses. It was found that NiFe and NiCu alloys were not formed, but the formation of NiZn and NiGa alloys was confirmed by XRD, HRTEM and XPS analyses. With increasing the Al content, the Ni particle size of Ni/AISBA-15 first decreased and then increased meaning that the Ni particle size can be tuned by controlling the doping of Al. All catalysts were evaluated and compared in terms of activity and selectivity in the semihydrogenation of phenylacetylene under very mild condition (40 °C and 0.1 MPa) in a semibatch stirred tank reactor. The results from monometallic Ni/AISBA-15(x) catalysts showed that the activity and selectivity relied on the Ni particle size: smaller Ni particles generally gave rise to higher initial rate but lower specific activity, while the selectivity to styrene first remained unchanged and then decreased with increasing the Ni particle size. These results indicate the structure-sensitive characteristic of the semihydrogenation of phenylacetylene over the Ni-based catalysts.

**Table 2**

Comparison of NiZn<sub>3</sub>/AISBA-15(40) with conventional catalysts in semihydrogenation of phenylacetylene<sup>a</sup>.

Catalysts	Reaction time (min)	Conversion (%)	Selectivity (%)
Pd/Al <sub>2</sub> O <sub>3</sub> <sup>b</sup>	80	99.5	47.8
Lindlar catalyst <sup>c</sup>	1800	99.3	90.2
Ni/Al <sub>2</sub> O <sub>3</sub> <sup>d</sup>	900	23.5	93.1
Ni/SiO <sub>2</sub> <sup>d</sup>	900	29.8	91.5
NiZn <sub>3</sub> /AISBA-15(40)	930	99.6	90.3

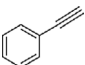
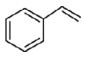
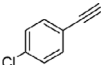
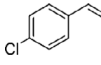
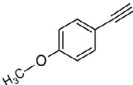
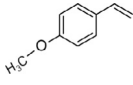
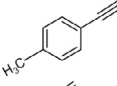
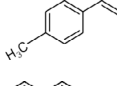
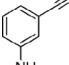
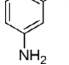
<sup>a</sup> Reaction condition: 40 °C, 0.1 MPa, 5 wt% phenylacetylene in methanol, in a semibatch stirred tank reactor.

<sup>b</sup> Prepared by impregnation method with a Pd loading of 0.5 wt% and reduced at 450 °C for 2 h.

<sup>c</sup> Purchased from Aladdin Reagent Int., with a Pd loading of 5 wt% poisoned by a lead complex.

<sup>d</sup> Prepared by the method used in this work, with a Ni loading of 10 wt%.

**Table 3**  
Semihydrogenation of various phenylacetylene derivatives over NiZn<sub>3</sub>/AISBA-15(40)<sup>a</sup>.

Reaction	Substrate	Desired product	Time (h)	Conversion (%)	Selectivity (%)
1			15.5	99.6	90.3
2			28.7	99.3	93.5
3			31.0	99.5	90.5
4			16.7	99.4	90.8
5			71.6	99.6	94.1

<sup>a</sup> Reaction condition: 40 °C, 0.1 MPa, 5 wt% substrate in methanol, in a semibatch stirred tank reactor.

The results from bimetallic Ni–M/AISBA-15 showed that NiZn and NiGa catalysts had higher selectivity as compared to NiCu and NiFe catalysts, which was mainly attributed to the geometric and electronic effects that were originated from the NiZn and NiGa alloys. DFT calculations also revealed that the adsorption energy of styrene on the NiZn alloy was much higher than that on metallic Ni, which in turn allowed the rapid desorption of styrene from the surface of NiZn alloy and prevented the over-hydrogenation. Among all the catalysts, NiZn<sub>3</sub>/AISBA-15(40) possessed the highest selectivity to styrene (90.3% at nearly 100% conversion of phenylacetylene), which was also superior to conventional catalysts including Pd/Al<sub>2</sub>O<sub>3</sub>, Ni/Al<sub>2</sub>O<sub>3</sub>, Ni/SiO<sub>2</sub> and Lindlar catalyst. When applied to the continuous hydrogenation of a model commercial C<sub>8</sub> fraction of pygas (2 wt% of phenylacetylene, 28 wt% of styrene, 30 wt% of ethylbenzene and 40 wt% of xylene), NiZn<sub>3</sub>/AISBA-15 (40) exhibited stable activity and high selectivity to styrene over 100 h of time on stream. Meanwhile, its structure is well maintained. In addition, this catalyst was capable of converting a majority of phenylacetylene derivatives into alkenyl aromatics with high selectivity. Therefore, the nonprecious NiZn<sub>3</sub>/AISBA-15(40) is a promising catalyst for the semihydrogenation of phenylacetylene and its derivatives.

## Acknowledgements

We gratefully acknowledge financial supports from the National Natural Science Foundation of China (21776088) and the Fundamental Research Funds for the Central Universities (222201718003).

## Appendix A. Supplementary material

Supplementary data to this article can be found online at <https://doi.org/10.1016/j.jcat.2019.01.012>.

## References

- [1] F.M. Lee, S.G. Norwood, J.C. Gentry, US Patent (1999) 5,877,385.
- [2] S.Q. Li, J.T. Liu, Z.Y. Zhu, J.H. Zhu, J. Kuai, U.S. Patent (2014) 8,916,736.
- [3] J.W. Hu, Z.M. Zhou, R. Zhang, L. Li, Z.M. Cheng, *J. Mol. Catal. A: Chem.* 381 (2014) 61–69.
- [4] Z. Zhou, J. Hu, R. Zhang, L. Li, Z. Cheng, *Chem. Eng. Sci.* 138 (2015) 663–672.
- [5] J.T. Merrill, US Patent (2004), 6,727,398.
- [6] M.B. Boucher, B. Zucig, G. Cladaras, J. Kammert, M.D. Marcinkowski, T.J. Lawton, E.C. Sykes, M. Flytzani-Stephanopoulos, *Phys. Chem. Chem. Phys.* 15 (2013) 12187–12196.
- [7] S.A. Nikolaev, L.N. Zhanavskina, V.V. Smirnov, V.A. Averyanov, K.L. Zhanavskina, *Russian Chem. Rev.* 78 (2009) 231–247.
- [8] P. Weerachawanasak, O. Mekasuwandumrong, M. Arai, S.I. Fujita, P. Prasertthadam, J. Panpranot, *J. Catal.* 262 (2009) 199–205.
- [9] M. Crespo-Quesada, F. Cárdenas-Lizana, A.L. Dessimoz, L. Kiwi-Minsker, *ACS Catal.* 2 (2012) 1773–1786.
- [10] L. Chen, B. Huang, X. Qiu, X. Wang, R. Luque, Y. Li, *Chem. Sci.* 7 (2016) 228–233.
- [11] Z. Wang, L. Yang, R. Zhang, L. Li, Z. Cheng, Z. Zhou, *Catal. Today* 264 (2016) 37–43.
- [12] L. Yang, X. Chen, Z. Zhou, R. Zhang, L. Li, Z. Cheng, X. Fang, *ChemistrySelect* 1 (2016) 5599–5606.
- [13] L. Yang, Y. Jin, X. Fang, Z. Cheng, Z. Zhou, *Ind. Eng. Chem. Res.* 56 (2017) 14182–14191.
- [14] V. Polshettiwar, B. Baruwati, R.S. Varma, *Green Chem.* 11 (2009) 127–131.
- [15] X. Chen, A. Zhao, Z. Shao, C. Li, C.T. Williams, C. Liang, *J. Phys. Chem. C* 114 (2010) 16525–16533.
- [16] X. Chen, M. Li, J. Guan, X. Wang, C.T. Williams, C. Liang, *Ind. Eng. Chem. Res.* 51 (2012) 3604–3611.
- [17] W. Donphai, T. Kamegawa, M. Chareonpanich, H. Yamashita, *Ind. Eng. Chem. Res.* 53 (2014) 10105–10111.
- [18] A.V. Erokhin, E.S. Lokteva, A.Y. Yermakov, D.W. Boukhvalov, K.I. Maslakov, E.V. Golubina, M.A. Uimin, *Carbon* 74 (2014) 291–301.
- [19] K. Yang, X. Chen, J. Guan, C. Liang, *Catal. Today* 246 (2015) 176–183.
- [20] E.V. Golubina, E.S. Lokteva, A.V. Erokhin, A.A. Veligzhanin, Y.V. Zubavichus, V.A. Likholobov, V.V. Lunin, *J. Catal.* 344 (2016) 90–99.
- [21] G. Wienhöfer, F.A. Westerhaus, R.V. Jagadeesh, K. Junge, H. Junge, M. Beller, *Chem. Commun.* 48 (2012) 4827–4829.
- [22] M. Pang, Z. Shao, X. Wang, C. Liang, *AlChE J.* 61 (2015) 2522–2531.
- [23] K. Yang, X. Chen, L. Wang, L. Zhang, S. Jin, C. Liang, *ChemCatChem* 9 (2017) 1–7.
- [24] X. Li, Y. Zhang, A. Wang, Y. Wang, Y. Hu, *Catal. Commun.* 11 (2010) 1129–1132.
- [25] Y. Chen, C. Li, J. Zhou, S. Zhang, D. Rao, S. He, M. Wei, D.G. Evans, X. Duan, *ACS Catal.* 5 (2015) 5756–5765.
- [26] G. Wowsnick, D. Teschner, M. Armbrüster, I. Kasatkin, F. Girgsdies, Y. Grin, R. Schlögl, M. Behrens, *J. Catal.* 309 (2014) 221–230.
- [27] C. Li, Y. Chen, S. Zhang, J. Zhou, F. Wang, S. He, M. Wei, D.G. Evans, X. Duan, *ChemCatChem* 6 (2014) 824–831.
- [28] Y. Liu, X. Liu, Q. Feng, D. He, L. Zhang, C. Lian, R. Shen, G. Zhao, Y. Ji, D. Wang, G. Zhou, Y. Li, *Adv. Mater.* 28 (2016) 4747–4754.
- [29] Y. Liu, J. Zhao, J. Feng, Y. He, Y. Du, D. Li, *J. Catal.* 359 (2018) 251–260.
- [30] A. Vinu, G.S. Kumar, K. Ariga, V. Murugesan, *J. Mol. Catal. A: Chem.* 235 (2005) 57–66.
- [31] P. Djinić, I.G.O. Črnivec, B. Erjavec, A. Pintar, *Appl. Catal. B: Environ.* 125 (2012) 259–270.
- [32] J. Xin, H. Cui, Z. Cheng, Z. Zhou, *Appl. Catal. A: Gen.* 554 (2018) 95–104.
- [33] A. Vinu, V. Murugesan, W. Böhlmann, M. Hartmann, *J. Phys. Chem. B* 108 (2004) 11496–11505.
- [34] G. Gutiérrez, B. Johansson, *Phys. Rev. B* 65 (104202) (2002) 1–9.
- [35] A. Fernández-Jiménez, A. Palomo, *Micropor. Mesopor. Mat.* 86 (2005) 207–214.
- [36] T. Simon, N. Bouchonville, M.J. Berr, A. Vaneski, A. Adrović, D. Volbers, R. Wyrwich, M. Döblinger, A.S. Susha, A.L. Rogach, F. Jäckel, J.K. Stolarczyk, J. Feldmann, *Nat. Mater.* 13 (2014) 1013–1018.
- [37] M.A. Lucchini, A. Testino, C. Ludwig, A. Kambolis, M. El-Kazzi, A. Cervellino, P. Riani, F. Canepa, *Appl. Catal. B* 156 (2014) 404–415.
- [38] S. Liu, K.H. Kim, J.M. Yun, A. Kundu, K.V. Sankar, U.M. Patil, C. Ray, S.C. Jun, *J. Mater. Chem. A* 5 (2017) 6292–6298.
- [39] S. Liu, K.S. Hui, K.N. Hui, H.F. Li, K.W. Ng, J. Xu, Z. Tang, S.C. Jun, *J. Mater. Chem. A* 5 (2017) 19046–19053.
- [40] A. Malki, Z. Mekhalif, S. Dettriche, G. Fonder, A. Boumaza, A. Djelloul, *J. Solid State Chem.* 215 (2014) 8–15.

- [41] S. Domínguez-Domínguez, Á. Berenguer-Murcia, Á. Linares-Solano, D. Cazorla-Amorós, J. Catal. 257 (2008) 87–95.
- [42] A. Yin, C. Wen, X. Guo, W.L. Dai, K. Fan, J. Catal. 280 (2011) 77–88.
- [43] F. Studt, F. Abild-Pedersen, T. Bligaard, R.Z. Sørensén, C.H. Christensen, J.K. Nørskov, Science 320 (2008) 1320–1322.
- [44] X. Yan, J. Sun, Y. Wang, J. Yang, J. Mol. Catal. A: Chem. 252 (2006) 17–22.
- [45] A. Petrauskas, L. Grincevičienė, A. Češūnienė, R. Juškėnas, Electrochim. Acta 50 (2005) 1189–1196.
- [46] E.M. de Oliveira, I.A. Carlos, Surf. Coat. Tech. 206 (2011) 250–256.
- [47] W.H. Chiang, R.M. Sankaran, Nat. Mater. 8 (2009) 882–886.
- [48] L. Wang, F. Li, Y. Chen, J. Chen, J. Energy Chem. 29 (2019) 40–49.
- [49] J.M. Yang, S.P. Gou, I.W. Sun, Chem. Commun. 46 (2010) 2686–2688.
- [50] B. Yoon, H.B. Pan, C.M. Wai, J. Phys. Chem. C 113 (2009) 1520–1525.
- [51] J. Qiu, H. Zhang, X. Wang, H. Han, C. Liang, C. Li, React. Kinet. Catal. Lett. 88 (2006) 269–276.
- [52] A. Yarulin, I. Yuranov, F. Cárdenas-Lizana, D.T.L. Alexander, L. Kiwi-Minsker, Appl. Catal. A: Gen. 478 (2014) 186–193.